MATHEMATICAL MODELING AND COMPUTING, Vol. 11, No. 2, pp. 555–570 (2024)

An exact solution for unsteady three-dimensional magnetohydrodynamic Casson flow of dusty nanofluid over a porous stretching sheet

Kopp M. I.[1], Yanovsky V. V.[1,2]

[1] *Institute for Single Crystals, NAS Ukraine, Nauka Ave. 60, Kharkiv 61072, Ukraine*
[2] *V. N. Karazin Kharkiv National University, 4 Svoboda Sq., Kharkiv 61022, Ukraine*

(Received 4 July 2023; Revised 23 June 2024; Accepted 24 June 2024)

The unsteady three-dimensional (3D) Casson flow of a nanofluid containing dust particles over a porous, linearly stretching sheet in the presence of an external magnetic field is studied. It is assumed that the sheet is stretched in both directions along the xy plane. The governing equations of the two-phase model are partial differential equations that are transformed into ordinary equations using similarity transforms. The nanofluid is a suspension of water-based nanoparticles. In this study, we look at how nanoparticle size affect the properties of dusty nanofluid flow. The mathematical model contains the basic equations for the fluid and dust phases in the form of three-dimensional partial differential equations, which are transformed into dimensionless ordinary-dimensional equations using an appropriate similarity transformation. An exact analytical solution to this boundary value problem is obtained. The effects of various physical values on dust and nanofluid velocities are discussed in detail, including the Casson parameter, magnetic parameter, porosity parameter, fluid-particle interaction parameter, mass concentration of dust particles, and nanoparticle size. In a few specific instances, the current analytical solution demonstrates a good agreement with previously published numerical investigations.

Keywords: *stretching sheet; unsteady three-dimensional (3D) Casson flow; nanofluid; dust particles; nanoparticles diameter; Lorentz force.*

2010 MSC: 76D05, 76D10, 76N20 **DOI:** 10.23939/mmc2024.02.555

1. Introduction

In the last decade, the problem of the boundary flow of non-Newtonian dusty fluids has attracted more and more attention. A dusty fluid (Newtonian or non-Newtonian) is a two-phase medium that consists of a continuous fluid and a discrete (solid) phase of particles. Dusty fluids are most commonly found in nature as atmospheric precipitation, near-earth plasma, and cosmic plasma. The flow of dusty fluid can also be observed in processes such as nuclear reactor cooling, powder technology, paint spraying, solid propellant nozzles, and guided missile emissions. All the phenomena listed above accelerated the consideration of modeling, solving, and analysing the flow of dusty fluids. As a result, new combined fluid models with rheological features, such as a dusty Casson nanofluid, have emerged to effectively describe complex technological processes.

The study of the laminar flow of a dusty Newtonian fluid was first carried out by Suffman [1]. Chakrabarti [2] studied the flow of dusty gas in the region of the boundary layer. The flow of a dusty liquid over a semi-infinite plate was discussed by Datta and Mishra [3]. The study of magnetohydrodynamic (MHD) flow is important due to numerous engineering applications such as reactor cooling, power generators, MHD pumps, the oil industry, and heat exchanger design. In addition, MHD flows play an important role in geophysics, astrophysics, solar physics, metrology, and the motion of the Earth's core. Given the significance of the MHD flow, many researchers began to investigate the hydromagnetic flows of a dusty fluid.

Vajravelu and Nayfeh [4] analysed the hydromagnetic flow of a dusty fluid over a stretching surface. Gireesha et al. [5] obtained a numerical solution for the two-dimensional flow in the boundary layer

and the heat transfer of a dusty fluid on the stretching surface. A numerical solution of the MHD flow and heat transfer of a dusty fluid over a linearly stretching sheet was given by Gireesha et al. [6]. Numerical investigations for the effect of thermal stratification on MHD flow and heat transfer of dusty fluid over a vertical stretching sheet embedded in a thermally stratified porous medium in the presence of uniform heat source and thermal radiation was conducted by Gireesha et al. [7].

Many processes use a wide range of fluids, such as saline solutions, melted sauce, toothpaste, molasses, dyes, blood, or shampoo, which have the remarkable property of being highly viscous. Newtonian fluids' fundamental theory of stress and strain rate cannot be applied to such fluids. One of the best models of non-Newtonian fluids is the Casson fluid, which exhibits yield strength, shear thinning, and high shear viscosity. The Casson model can also behave like a Newtonian fluid when the surface stress is significantly greater than the yield strength or when there is a very high shear stress on the wall.

Sakiadis [8] and Tsou et al. [9] were among the first to investigate boundary layer flow on solid surfaces. Crane [10] found an analytical solution for a two-dimensional stationary flow in a boundary layer caused by an expanding surface whose velocity varies linearly with distance from a fixed point. Numerous researchers have been motivated by these papers [8–10] to investigate various aspects of this problem, whether by combining the problem with heat and mass transfer, MHD, chemical processes, suction/injection, mass transpiration, non-Newtonian fluids, or other different scenarios. Studies on two-dimensional boundary layer flow caused by stretching surfaces are extensively studied with various fluids under different conditions due to their numerous applications. For a long time, there have been a large number of articles published about this topic. As a result, the articles that discuss three-dimensional MHD flows of a non-Newtonian (Casson) fluid over a stretching or contracting surface will be the primary focus of the review section of this study.

Bhattacharyya [11] considered the two-dimensional magnetohydrodynamic stagnation-point flow and heat transfer of an electrically conducting non-Newtonian Casson fluid towards a stretching sheet in the presence of thermal radiation. Mukhopadhyay et al. [12] investigated the unsteady two dimensional flow of a non-Newtonian fluid over a stretching surface with a prescribed surface temperature. Nandy [13] investigated the hydromagnetic boundary layer flow and heat transfer of a non-Newtonian Casson fluid in the neighborhood of a stagnation point over a stretching sheet in the presence of velocity and thermal slip at the boundary. Nadeem et al. [14] investigated the Casson fluid flow on a permeable sheet caused by sheet stretching in the x and y directions in a transverse magnetic field. In a later study, Nadeem et al. [15] extended the study to a Casson nanofluid over a linearly stretching sheet, taking into account surface convective conditions. Mahanta and Shaw [16] investigated a three-dimensional Casson fluid flow past a porous linearly stretching sheet, introducing a convective boundary condition at the surface where the fluid's thermal conductivity varies linearly concerning temperature. They used the Spectral Relaxation Method (SRM) to solve the governing equations, and computations were performed for the velocity and temperature fields for different parameters. Krishna [17] solved MHD Casson fluid flow past a porous, linearly stretching surface with wall mass transfer analytically. In [17] the fluid velocity and skin friction coefficient were calculated, and it was demonstrated that increasing the Casson and porosity parameters suppressed the velocity field.

A colloidal suspension of a nanoscale particle in a basic fluid is known as a "nanofluid" [18]. Metals, oxides, carbides, and carbon nanotubes are among the most commonly used nanoparticles, with water and ethylene glycol serving as the base fluids. For the effective transmission of thermal energy, nanofluids have a higher thermal conductivity than ordinary fluids. A suspension of nanosized particles can affect the viscous and rheological properties of a nanofluid since an increase in the volume fraction of nanoparticles increases the dynamic viscosity. Oyelakin et al. [19] investigated the effects of thermal radiation, heat, and mass transfer on the unsteady magnetohydrodynamic (MHD) flow of a three-dimensional Casson nanofluid. In [19], the influence of porosity, the magnetic field, and the stretching degree parameter on the flow of the Casson nanofluid model over a porous, linearly stretching sheet with the inclusion of nanoparticles on the concentration boundary condition was shown. It was found

that an increase in flow unsteadiness tends to decrease momentum, heat flow, and nanoparticle volume fraction profiles [19]. Madhusudan et al. [20] numerically studied the convective, three-dimensional, electrically conducting Casson nanofluid flow over an exponentially stretching sheet embedded in a saturated porous medium and subjected to thermal as well as solute slip in the presence of an externally applied transverse magnetic field. Ibrahim and Anbessa [21] investigated the three-dimensional MHD mixed convection flow of Casson nanofluid over an exponentially stretching sheet using the impacts of Hall and ion slip currents, taking into account thermal radiation and the heat source. Recently, Japili et al. [22] investigated numerically MHD stagnation point flow over a stretching or shrinking sheet in a porous medium with velocity slip. It was found that the coefficient of surface friction and the local Nusselt number increase with increasing magnetic and permeability parameters. Yahaya et al. [23] studied numerical solutions for the flow of Ag-CuO/H_2O hybrid nanofluid on a stretchable sheet with the effects of suction, magnetic field, double stratification, and sliding. It has been established that an increase in the sliding and stratification parameters of solutions leads to a decrease in the Sherwood number. At the same time, an increase in the parameters of thermal slip and stratification reduces the Nusselt number. An increase in the skin friction coefficient is observed with an increase in the hydrodynamic slip parameter. Alias and Hafidzuddin [24] considered a magnetohydrodynamic(MHD) induced Navier slip flow over a non-linear stretching and shrinking sheet with the existence of suction. The findings in [24] demonstrated that, in contrast to the shrinking case, the range of dual solutions for a stretched sheet is smaller, and that suction increases skin friction while the slip parameter decreases shear wall stress. Nithya and Vennila [25] investigated the steady incompressible two-dimensional hydromagnetic boundary layer flow of nanofluid passing through a stretched sheet in the influence of viscous and ohmic dissipations. A semi-analytical technique known as the DTM-Pade Approximation was employed to solve the problem. The authors [25] displayed a stronger trend in the velocity profile for the nonlinear stretching parameter n, suction S, and magnetics M parameters. When the Prandtl number rises, however, the opposite trend is observed in relation to the temperature profile. The concentration profile exhibits increasing behavior for the Lewis number and other parameters.

The literature mentioned above indicates that the majority of investigations are based on numerical solutions. An accurate analytical solution has the advantage of being able to describe the physics of fluid flow. The accurate answer may also be used as a benchmark for further numerical and approximative studies. Jalil et al. [26] gave an exact analytical solution for the MHD boundary flow of a dusty liquid over an extension surface. The mathematical methodology used in [26] consists of transforming the basic equations into a self-similar form using known similarity transformations. The coupled equations are then analytically solved using Crane's [10] solution as a guide. Vishalakshi et al. [27] obtained exact analytical solutions for the three-dimensional flow of a non-Newtonian fluid due to a porous stretching/shrinking sheet. The importance of paper [27] is to examine the problem analytically and find the domain in terms of mass transpiration that is used in the heat transfer equation to analyze the heat equation. Mahabaleshwar et al. [28] conducted an investigation of the exact analytical solution for velocity and concentration field for 3D MHD flow viscoelastic HNF due to a porous sheet that stretched/shrunk along both x and y axes with linear velocity and Navier slip. Exact analytical solutions in exponential and hypergeometric form for velocity and concentration fields were obtained in [28]. The flow of Marangoni convection MHD Casson fluid with carbon nanotubes under the effects of transpiration and radiation was analyzed by Vishalakshi et al. [29]. The ordinary differential equations (ODEs) obtained in [29] are solved analytically, first using the momentum equation to obtain the solution domain, and then using this domain, the energy equation is solved to obtain the temperature profile in terms of the Laguerre polynomial. Recently, Khan et al. [30] found an exact solution of a Casson fluid flow induced by dust particles with hybrid nanofluid over a stretching sheet under a Lorentz force. They obtained the analytical solutions of momentum equations for the fluid and dust phases velocities of the normal nanofluid (Fe_3O_4/H_2O) and hybrid nanofluid (Fe_3O_4-MWCNT/H_2O).

The above review of the literature on this topic showed that most studies are based on numerical solutions. Unlike the previous numerical [19] and analytical [26, 30] works, this work is devoted to

an analytical study of the three-dimensional MHD Casson flow of a dusty nanofluid due to stretching of a porous surface. In this study, we will apply a methodology based on Crane's exact analytical solutions. In addition, the novelty of this study is to explain how the size of nanoparticles affects the properties of a dusty nanofluid flow. Using various physical parameters, an exact check of the problem is performed, and velocity profiles and skin friction coefficients in the x and y directions are studied. The results of this work can be applied to numerous technological processes where it is important to take the non-stationarity of the flow into account.

2. Basic equations and boundary conditions

Consider an unsteady three-dimensional laminar, incompressible Casson nanofluid flow over a linearly stretching porous sheet. The unsteady fluid flow begins at $t = 0$ and has linear stretching velocities $U_w = ax/(1 - \lambda t)$ and $V_w = by/(1 - \lambda t)$ along the x and y-planes, where a, b and λ are positive constants. It should be noted that the expressions U_w, V_w are only applicable for $t < 1/\lambda$. As seen in Figure 1, the fluid is positioned along the z-axis, and a variable magnetic field $B(t) = B_0/\sqrt{1 - \lambda t}$ is applied perpendicular to the direction of the flow, where B_0 is the constant intensity of a magnetic field. The induced magnetic field is supposed to be insignificant in comparison to the weak applied magnetic field. Additionally, uniform size, constant density, and spherical shape are expected characteristics of dust particles. An isotropic, incompressible Casson fluid's rheological equation has the following structure (see, for example, [12]):

$$\tau_{ij} = \begin{cases} 2\left(\mu + \frac{P_y}{\sqrt{2\pi}}\right) e_{ij}, & \pi > \pi_c, \\ 2\left(\mu + \frac{P_y}{\sqrt{2\pi_c}}\right) e_{ij}, & \pi < \pi_c, \end{cases} \tag{1}$$

$$e_{ij} = \frac{1}{2}\left(\frac{\partial v_i}{\partial x_j} + \frac{\partial v_j}{\partial x_i}\right),$$

where τ_{ij} is the $(i,j)^{\text{th}}$ component of the stress tensor, μ is the dynamic viscosity of a viscoplastic fluid, P_y is the yield stress of the fluid, $\pi = e_{ij}e_{ij}$ is the product of the component of deformation rate with itself, e_{ij} is the $(i,j)^{\text{th}}$ component of deformation rate, and π_c is the critical value of π depends on non-Newtonian model.

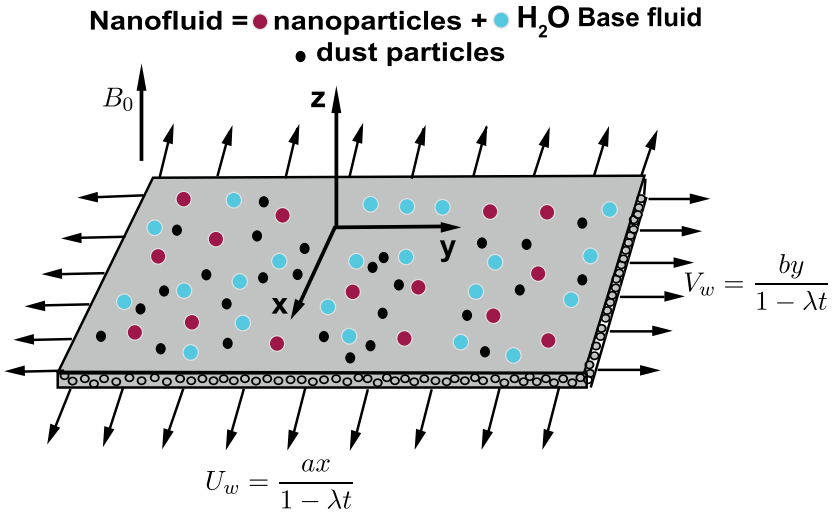

Fig. 1. Schematic diagram for the three-dimensional unsteady flow problem.

The governing equations for the flow and dusty fluid under the boundary-layer approximations and the aforementioned assumptions are as follows.
For the fluid phase:

$$\frac{\partial u}{\partial x} + \frac{\partial v}{\partial y} + \frac{\partial w}{\partial z} = 0, \tag{2}$$

$$\frac{\partial u}{\partial t}+u\frac{\partial u}{\partial x}+v\frac{\partial u}{\partial y}+w\frac{\partial u}{\partial z}=\frac{\mu_{nf}}{\rho_{nf}}\left(1+\frac{1}{\Lambda}\right)\frac{\partial^2 u}{\partial z^2}-\frac{\mu_{nf}}{\widetilde{k}\rho_{nf}}u-\frac{\sigma_{nf}}{\rho_{nf}}B^2u+\frac{KN}{\rho_{nf}}(u_p-u), \tag{3}$$

$$\frac{\partial v}{\partial t}+u\frac{\partial v}{\partial x}+v\frac{\partial v}{\partial y}+w\frac{\partial v}{\partial z}=\frac{\mu_{nf}}{\rho_{nf}}\left(1+\frac{1}{\Lambda}\right)\frac{\partial^2 v}{\partial z^2}-\frac{\mu_{nf}}{\widetilde{k}\rho_{nf}}v-\frac{\sigma_{nf}}{\rho_{nf}}B^2v+\frac{KN}{\rho_{nf}}(v_p-v). \tag{4}$$

For the dust phase:

$$\frac{\partial u_p}{\partial x}+\frac{\partial v_p}{\partial y}+\frac{\partial w_p}{\partial z}=0, \tag{5}$$

$$\frac{\partial u_p}{\partial t}+u_p\frac{\partial u_p}{\partial x}+v_p\frac{\partial u_p}{\partial y}+w_p\frac{\partial u_p}{\partial z}=\frac{KN}{\rho_p}(u-u_p), \tag{6}$$

$$\frac{\partial v_p}{\partial t}+u_p\frac{\partial v_p}{\partial x}+v_p\frac{\partial v_p}{\partial y}+w_p\frac{\partial v_p}{\partial z}=\frac{KN}{\rho_p}(v-v_p), \tag{7}$$

where (u,v,w) and (u_p,v_p,w_p) are the velocities of nanofluid and dust particles along the x, y, and z-directions. Next, ρ_{nf}, μ_{nf}, σ_{nf} are the density, dynamic viscosity, and electrical conductivity of nanofluid, respectively. Λ is the Casson (non-Newtonian) fluid parameter, $\widetilde{k}$ is the permeability of a porous medium. $K=6\pi\mu_f r$ is Stokes drag constant, r is radius of dust particles, N and ρ_p are the dust particle number and the density of the dust particle, respectively.

The boundary conditions are

$$u=U_w(x)=\frac{ax}{1-\lambda t},\quad v=V_w(y)=\frac{by}{1-\lambda t},\quad w=0\quad\text{at}\quad z=0, \tag{8}$$

$$u=u_p\to 0,\quad v=v_p\to 0,\quad w=w_p\quad\text{at}\quad z\to\infty. \tag{9}$$

The subscript "nf" denotes the physical quantities for the nanofluid in equations (3)–(4) and are defined as follows [31]:

- Dynamic viscosity

$$\varepsilon_1=\frac{\mu_{nf}}{\mu_f}=1+2.5\phi_s+4.5\left[\frac{h}{d_n}\left(2+\frac{h}{d_n}\right)\left(1+\frac{h}{d_n}\right)^2\right]^{-1}; \tag{10}$$

- Density

$$\varepsilon_2=\frac{\rho_{nf}}{\rho_f}=1-\phi_s+\phi_s\frac{\rho_s}{\rho_f}; \tag{11}$$

- Electrical conductivity

$$\varepsilon_3=\frac{\sigma_{nf}}{\sigma_f}=1+\frac{3\phi_s\left(\frac{\sigma_s}{\sigma_f}-1\right)}{\left(\frac{\sigma_s}{\sigma_f}+2\right)-\phi_s\left(\frac{\sigma_s}{\sigma_f}-1\right)}, \tag{12}$$

where ϕ_s is the nanoparticle concentration, d_n depicts the nanoparticle's diameter, and h is the inter-particle distance. Next, ρ_f is the base fluid density, ρ_s is density of nanoparticle, σ_f depicts the electric conductance of the base fluid, and σ_s is the electric conductance of nanoparticle. Table 1 shows the physical characteristics of some types of nanofluids.

Table 1. Physical properties of the nanoparticles and the base fluid.

Property	H_2O	Cu
ρ [kg·m^{-3}]	997.1	8933
σ [S·m^{-1}]	$5.5\cdot10^{-6}$	$5.96\cdot10^{7}$

We present the corresponding similarity transformations below:

$$u=\frac{axf'(\eta)}{1-\lambda t},\quad u_p=\frac{axF'(\eta)}{1-\lambda t},\quad v=\frac{ayg'(\eta)}{1-\lambda t},\quad v_p=\frac{ayG'(\eta)}{1-\lambda t},$$

$$w=-\sqrt{\frac{a\nu_f}{1-\lambda t}}(f(\eta)+g(\eta)),\quad w_p=-\sqrt{\frac{a\nu_f}{1-\lambda t}}(F(\eta)+G(\eta)),\quad \eta=z\sqrt{\frac{a}{\nu_f(1-\lambda t)}}, \tag{13}$$

where f, g, F, G are the dimensionless functions, η is the similarity variable, ν_f is the kinematic viscosity of the base fluid. Primes denote differentiation with regard to η in this context. Dimensionless equations for the fluid and dust phases are obtained by applying Eq. (2) to Eqs. (3)–(4) and (6)–(7):

$$\left(1+\frac{1}{\Lambda}\right)\frac{\varepsilon_1}{\varepsilon_2}f'''-\alpha_0\left(f'+\frac{\eta}{2}f''\right)+(f+g)f''-f'^2-\left(\frac{\varepsilon_3}{\varepsilon_2}M+\frac{\varepsilon_1}{\varepsilon_2}\widetilde{K}\right)f'+\frac{\beta_v l}{\varepsilon_2}(F'-f')=0, \quad (14)$$

$$\left(1+\frac{1}{\Lambda}\right)\frac{\varepsilon_1}{\varepsilon_2}g'''-\alpha_0\left(g'+\frac{\eta}{2}g''\right)+(f+g)g''-g'^2-\left(\frac{\varepsilon_3}{\varepsilon_2}M+\frac{\varepsilon_1}{\varepsilon_2}\widetilde{K}\right)g'+\frac{\beta_v l}{\varepsilon_2}(G'-g')=0, \quad (15)$$

$$F'^2-(F+G)F''+\alpha_0\left(F'+\frac{\eta}{2}F''\right)-\beta_v(f'-F')=0, \quad (16)$$

$$G'^2-(F+G)G''+\alpha_0\left(G'+\frac{\eta}{2}G''\right)-\beta_v(g'-G')=0. \quad (17)$$

The continuity equations (2) and (5) is automatically satisfied by using Eq. (2). Boundary conditions (8)–(9) are also transformed into the dimensionless form:

$$f(0)=0,\quad f'(0)=1,\quad g(0)=0,\quad g'(0)=c\quad\text{at}\quad\eta=0, \quad (18)$$

$$f'(\eta)\to 0,\quad g'(\eta)\to 0,\quad f(\eta)\to F(\eta),\quad g(\eta)\to G(\eta)\quad\text{at}\quad\eta\to\infty. \quad (19)$$

Dimensionless quantities

$$\alpha_0=\frac{\lambda}{a},\quad M=\frac{B_0^2\sigma_f}{a\rho_f},\quad \widetilde{K}=\frac{\nu_f(1-\lambda t)}{a\widetilde{k}},\quad \beta_v=\frac{KN}{a\rho_p}(1-\lambda t),\quad l=\frac{\rho_p}{\rho_f},\quad c=\frac{b}{a}$$

are defined as the unsteadiness parameter, the magnetic parameter, the porosity parameter, the momentum dust parameter, the mass concentration of dust particles parameter, the stretching ratio parameter, respectively.

The calculation of the skin friction coefficient C_f is very interesting for engineering problems. As a result, we will use local wall shear stresses τ_w to define the skin friction coefficient in directions x and y of the coordinates:

$$C_{fx}=\frac{\tau_{wx}}{\rho_f U_w^2},\quad C_{fy}=\frac{\tau_{wy}}{\rho_f U_w^2}. \quad (20)$$

The wall shear stresses along the x and y directions are denoted by

$$\tau_{wx}=\mu_{nf}\left(1+\frac{1}{\Lambda}\right)\left(\frac{\partial u}{\partial z}\right)_{z=0},\quad \tau_{wy}=\mu_{nf}\left(1+\frac{1}{\Lambda}\right)\left(\frac{\partial v}{\partial z}\right)_{z=0}.$$

Thus, the skin friction coefficients C_f along the x and y axes are expressed as follows:

$$C_{fx}\sqrt{\mathrm{Re}_x}=\frac{\mu_{nf}}{\mu_f}\left(1+\frac{1}{\Lambda}\right)f''(0),\quad C_{fy}\sqrt{\mathrm{Re}_x}=\frac{\mu_{nf}}{\mu_f}\left(1+\frac{1}{\Lambda}\right)\left(\frac{y}{x}\right)g''(0), \quad (21)$$

where $\mathrm{Re}_x=U_w x/\nu_f$ is the local Reynolds number. The exact analytical solution to equations (14)–(17) will be presented in the following section.

3. Exact analytical solution

Before beginning the process of determining the exact analytical solution of equations (14)–(17), we introduce additional similarity variables

$$f(\eta)\to\widetilde{f}(\eta)+\frac{\alpha_0\eta}{4},\quad F(\eta)\to\widetilde{F}(\eta)+\frac{\alpha_0\eta}{4},$$
$$g(\eta)\to\widetilde{g}(\eta)+\frac{\alpha_0\eta}{4},\quad G(\eta)\to\widetilde{G}(\eta)+\frac{\alpha_0\eta}{4}, \quad (22)$$

and as a result of their application, we obtain simplified equations (14)–(17):

$$\alpha_1\widetilde{f}'''-\widetilde{f}'^2+(\widetilde{f}+\widetilde{g})\widetilde{f}''-\left(\frac{3\alpha_0}{2}+\alpha_2\right)\widetilde{f}'-\frac{5\alpha_0^2}{16}-\frac{\alpha_0\alpha_2}{4}+\alpha_3(\widetilde{F}'-\widetilde{f}')=0, \quad (23)$$

$$\alpha_1\widetilde{g}'''-\widetilde{g}'^2+(\widetilde{f}+\widetilde{g})\widetilde{g}''-\left(\frac{3\alpha_0}{2}+\alpha_2\right)\widetilde{g}'-\frac{5\alpha_0^2}{16}-\frac{\alpha_0\alpha_2}{4}+\alpha_3(\widetilde{G}'-\widetilde{g}')=0, \quad (24)$$

$$\widetilde{F}'^2 - (\widetilde{F}+\widetilde{G})\widetilde{F}'' + \frac{3\alpha_0}{2}\widetilde{F}' + \frac{5\alpha_0^2}{16} - \beta_v(\widetilde{f}' - \widetilde{F}') = 0, \tag{25}$$

$$\widetilde{G}'^2 - (\widetilde{F}+\widetilde{G})\widetilde{G}'' + \frac{3\alpha_0}{2}\widetilde{G}' + \frac{5\alpha_0^2}{16} - \beta_v(\widetilde{g}' - \widetilde{G}') = 0, \tag{26}$$

where

$$\alpha_1 = \left(1+\frac{1}{\Lambda}\right)\frac{\varepsilon_1}{\varepsilon_2}, \quad \alpha_2 = \frac{\varepsilon_3}{\varepsilon_2}M + \frac{\varepsilon_1}{\varepsilon_2}\widetilde{K}, \quad \alpha_3 = \frac{\beta_v l}{\varepsilon_2}.$$

Boundary conditions (17)–(18) for new variables take the form

$$\widetilde{f}(0) = 0, \quad \widetilde{f}'(0) = 1 - \frac{\alpha_0}{4}, \quad \widetilde{g}(0) = 0, \quad \widetilde{g}'(0) = c - \frac{\alpha_0}{4} \quad \text{at} \quad \eta = 0, \tag{27}$$

$$\widetilde{f}'(\eta) \to -\frac{\alpha_0}{4}, \quad \widetilde{g}'(\eta) \to -\frac{\alpha_0}{4}, \quad \widetilde{f}(\eta) \to \widetilde{F}(\eta), \quad \widetilde{g}(\eta) \to \widetilde{G}(\eta) \quad \text{at} \quad \eta \to \infty. \tag{28}$$

We assume the exact solutions of equations (14)–(17) in exponential form:

$$\widetilde{f}(\eta) = A_1 + A_2 e^{-\beta\eta}, \quad \widetilde{g}(\eta) = A_3 + A_4 e^{-\beta\eta},$$
$$\widetilde{F}(\eta) = A_5 + A_6 e^{-\beta\eta}, \quad \widetilde{G}(\eta) = A_7 + cA_8 e^{-\beta\eta}, \tag{29}$$

where A_1, A_2, A_3, A_4, A_5, A_6, A_7, A_8 are the arbitrary constants. Applying the boundary conditions (27)–(28) to the solutions (3), we derive expressions for the coefficients as follows:

$$A_1 = \frac{1}{\beta}\left(1-\frac{\alpha_0}{4}\right), \quad A_2 = -\frac{1}{\beta}\left(1-\frac{\alpha_0}{4}\right), \quad A_3 = \frac{4c-\alpha_0}{4\beta},$$
$$A_4 = -\frac{4c-\alpha_0}{4\beta}, \quad A_5 = A_1 = \frac{1}{\beta}\left(1-\frac{\alpha_0}{4}\right), \quad A_7 = A_3 = \frac{4c-\alpha_0}{4\beta}. \tag{30}$$

The next step is to substitute solutions (3)–(3) into equations (23)–(24) to determine the coefficients A_6 and A_8. As a result, we arrive at the equation shown below for A_6 and A_8:

$$(1-c)(\alpha_1\beta^2 - 1 - c - \alpha_0 - \alpha_2 - \alpha_3) - \alpha_3\beta(A_6 - cA_8) = 0. \tag{31}$$

Substituting solutions (3)–(3) into equations (25)–(26), we get

$$A_6 - cA_8 = -\frac{\beta_v(1-c)}{\beta(1+c+\alpha_0+\beta_v)}, \tag{32}$$

here

$$A_6 = -\frac{\beta_v}{\beta(1+\alpha_0+\beta_v)}, \quad cA_8 = -\frac{c\beta_v(2+\alpha_0+\beta_v)}{\beta(1+\alpha_0+\beta_v)(1+c+\alpha_0+\beta_v)}.$$

From expressions (31) and (32), one can easily find the value β:

$$\beta = \pm\sqrt{\frac{1}{\alpha_1}\left(1+c+\alpha_0+\alpha_2+\alpha_3 - \frac{\alpha_3\beta_v}{1+c+\alpha_0+\beta_v}\right)}. \tag{33}$$

It is clear, we only need positive values of $\beta > 0$. Expressions (32)–(33) coincide with the result of the paper [30] in the limiting case for two-dimensional and steady flow: $c \to 0$, $\alpha_0 \to 0$. Finally, by substituting the values of the coefficients from (3) and (32) into expressions (3) and taking into account (3), we obtain the final form of exact analytical solutions for the fluid and dust phases:

$$f(\eta) = \frac{\alpha_0\eta}{4} + \left(\frac{4-\alpha_0}{4\beta}\right)\left(1-e^{-\beta\eta}\right), \quad g(\eta) = \frac{\alpha_0\eta}{4} + \left(\frac{4c-\alpha_0}{4\beta}\right)\left(1-e^{-\beta\eta}\right),$$
$$F(\eta) = \frac{\alpha_0\eta}{4} + \frac{1}{\beta}\left(1 - \frac{\alpha_0}{4} - \frac{\beta_v e^{-\beta\eta}}{1+\alpha_0+\beta_v}\right),$$
$$G(\eta) = \frac{\alpha_0\eta}{4} + \frac{1}{\beta}\left(c - \frac{\alpha_0}{4} - \frac{\beta_v(2+\alpha_0+\beta_v)e^{-\beta\eta}}{(1+\alpha_0+\beta_v)(1+c+\alpha_0+\beta_v)}\right). \tag{34}$$

By differentiating expressions (34) with respect to η, we can easily determine the velocity profiles in the x and y directions for the fluid and dust phases:

$$f'(\eta) = \frac{\alpha_0}{4} + \left(\frac{4-\alpha_0}{4}\right)e^{-\beta\eta}, \quad g'(\eta) = \frac{\alpha_0}{4} + \left(\frac{4c-\alpha_0}{4}\right)e^{-\beta\eta},$$

$$F'(\eta) = \frac{\alpha_0}{4} + \frac{\beta_v e^{-\beta\eta}}{1+\alpha_0+\beta_v}, \quad G'(\eta) = \frac{\alpha_0}{4} + \frac{c\beta_v(2+\beta_v)e^{-\beta\eta}}{(1+\alpha_0+\beta_v)(1+c+\alpha_0+\beta_v)}. \tag{35}$$

Differentiating expressions (3) by variable η determines the expressions $-f''(0)$ and $-g''(0)$, which are necessary for calculating skin friction coefficients of the fluid phase in both lateral directions:

$$-f''(0) = \left(\frac{4-\alpha_0}{4}\right)\beta, \quad -g''(0) = \left(\frac{4c-\alpha_0}{4}\right)\beta. \tag{36}$$

Table 2. A comparison of exact solutions for skin friction coefficients $-f''(0)$ and $-g''(0)$ with numerical results [19, 32–34].

Λ	M	c	$-f''(0)$ num. res.	$-g''(0)$ num. res.	$-f''(0)$ ex. sol.	$-g''(0)$ ex. sol.
∞	0	0	1.0000 [34]	0	1.0000	0
∞	0	0	1.0042 [32, 33]	0	1.0000	0
1	0	0	0.7071 [34]	0	0.7071	0
2	0	0	0.8164 [34]	0	0.8164	0
3	0	0	0.8660 [34]	0	0.8660	0
4	0	0	0.8944 [34]	0	0.8944	0
∞	0	0.5	1.0932 [32, 33]	0.4653 [32, 33]	1.2247	0.6123
∞	10	0.5	3.3420 [32, 33]	1.6459 [32, 33]	3.3911	1.6955
∞	100	0.5	10.058 [32, 33]	5.0208 [32, 33]	10.074	5.0373
1	10	0	2.3452 [19]	0	2.3452	0
1	10	0.5	2.3631 [19]	1.1638 [19]	2.3979	1.1989
5	10	0	3.0276 [19]	0	3.0276	0
5	10	0.5	3.0508 [19]	1.5025 [19]	3.0956	1.5478

4. Results and discussion

In this section, we discuss the results obtained from the exact analytical solution (33)–(34) for the unsteady flow of a nanofluid (Cu-H_2O) of dust particles in both lateral directions. Influence of the non-Newtonian (Cassonian) parameter Λ, the magnetic parameter M, the porosity parameter $\widetilde{K}$, the fluid particle interaction parameter β_v, and the mass concentration of dust particles l on nanofluid velocity profiles $f'(\eta)$, $g'(\eta)$ and dust velocity profiles $F'(\eta)$, $G'(\eta)$ are shown in Figures 2–8. For calculations, the range of variations of the following variables is considered:

$$\Lambda = (1, 3, \infty), \quad M = (0.5, 1.5, 2.5), \quad \widetilde{K} = (0.5, 1.5, 2.5),$$
$$\beta_v = (0.3, 0.5, 1), \quad l = (2, 3, 4), \quad d_n = (0.2, 1.2, 2.2), \quad c = 0.5,$$
$$\phi_s = 0.05, \quad h = 1, \quad \alpha_0 = 0.8.$$

Figures 2–4 show the effect of Λ, M and $\widetilde{K}$ on the fluid phase and dust phase velocities of nanofluid Cu-H_2O. These figures demonstrate that when the values of the parameters Λ, M and $\widetilde{K}$ grow, the velocities of the fluid and dust phases will continue to decrease. The physical meaning of the speed deceleration shown in Figure 2 is to increase the plastic dynamic viscosity due to the increase in the values of Λ, which creates resistance to the flowing fluid.

A similar behaviour of velocity profiles can be seen in Figure 3, which shows that the Lorentz force increases in accordance with the increase in the values of the magnetic parameter M. As a result, there is some resistance to the fluid flow, which leads to a decrease in the flow velocity profiles.

Figure 4 depicts that as the value of the porosity parameter $\widetilde{K}$ in the boundary layer increases, the velocities decrease in both directions. Therefore, the thickness of the boundary layer also decreases at higher values of $\widetilde{K}$.

Figure 5 illustrates the effect of the fluid interaction parameter β_v on the velocity of the fluid and dust phases for nanofluid (Cu-H_2O) as a function of η, respectively. These figures (Figures 5a, 5b, and 5c) show that as increases β_v, the velocities of the fluid phase $f'(\eta)$, $g'(\eta)$ decrease in both lateral

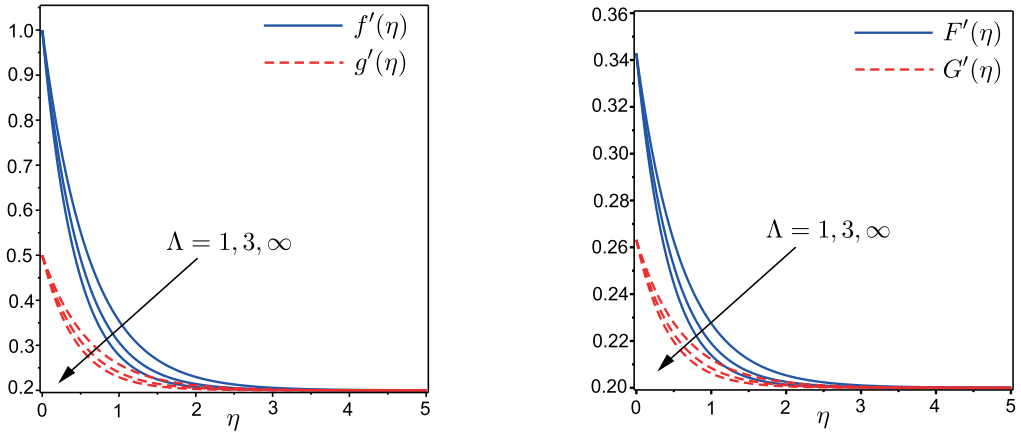

a ***b***

Fig. 2. Influence of Λ on velocity profiles $f'(\eta)$, $g'(\eta)$ and $F'(\eta)$, $G'(\eta)$ at fixed parameters $M = \widetilde{K} = c = 0.5$, $l = 2$, $d_n = 0.2$, $\alpha_0 = 0.8$, $h = 1$ and $\beta_v = 0.3$.

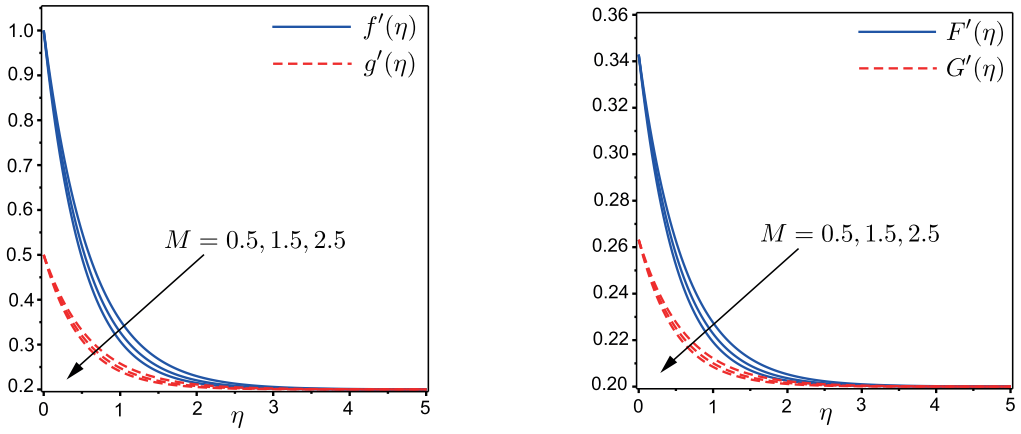

a ***b***

Fig. 3. Effect of M on velocity profiles $f'(\eta)$, $g'(\eta)$ and $F'(\eta)$, $G'(\eta)$ at fixed parameters $\Lambda = 1$, $\widetilde{K} = c = 0.5$, $l = 2$, $d_n = 0.2$, $\alpha_0 = 0.8$, $h = 1$ and $\beta_v = 0.3$.

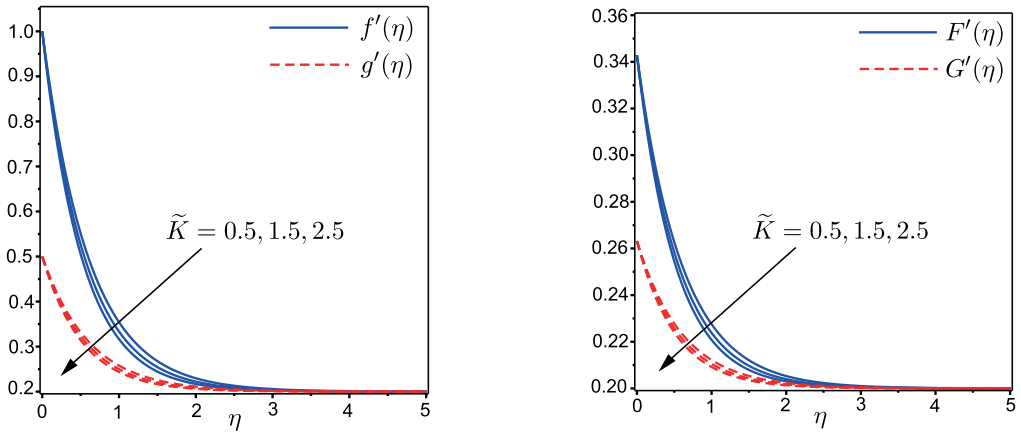

a ***b***

Fig. 4. Effect of $\widetilde{K}$ on velocity profiles $f'(\eta)$, $g'(\eta)$ and $F'(\eta)$, $G'(\eta)$ at fixed parameters $\Lambda = 1$, $M = c = 0.5$, $l = 2$, $d_n = 0.2$, $\alpha_0 = 0.8$, $h = 1$ and $\beta_v = 0.3$.

directions x and y, while the velocities of the dust phase $F'(\eta)$, $G'(\eta)$ increase. This is due to the fact that a larger fluid interaction parameter β_v creates more resistance for the fluid flow phase and less for the dust phase.

The impact of l on the fluid phase and dust phase velocities for the nanofluid (Cu-H_2O)is shown in Figure 6. This demonstrates that a decrease in the velocity profiles for both the fluid and dust phases is caused by an increase in the parameter l. This is because an increase in the parameter l directly correlates with an increase in dust particle density. The result is an increase in the flow resistance for both the fluid and dust phases.

The effect of an increase in the nanoparticle diameter d_n on the velocity profiles for the fluid and dust phases is shown in Figure 7. Hence, we see that as the nanoparticle diameter d_n increases, the flows for the fluid and dust phases accelerate in the lateral directions x and y, as a result, the thickness of the boundary layer also increases.

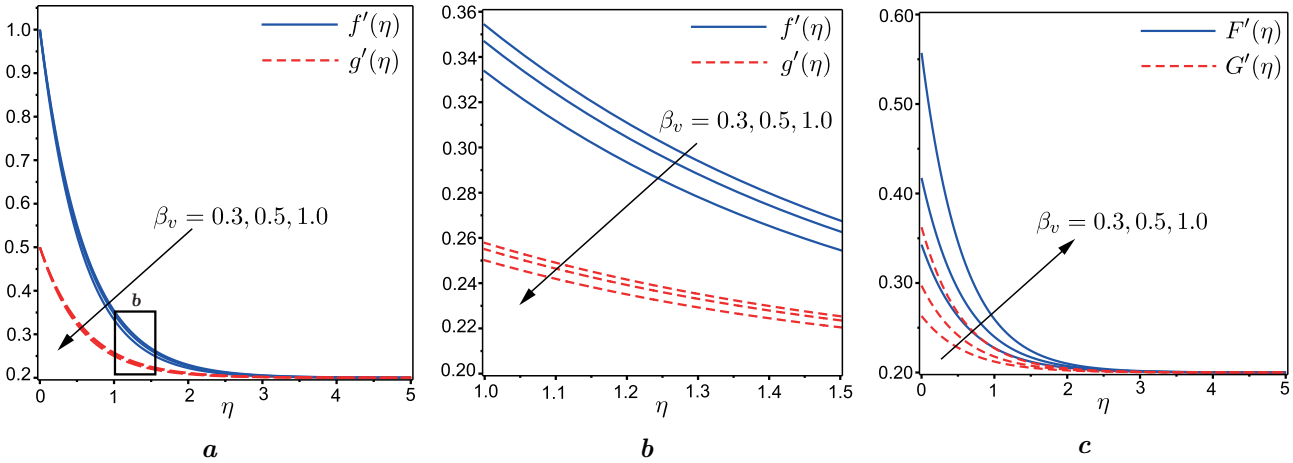

Fig. 5. Influence of β_v on velocity profiles $f'(\eta)$, $g'(\eta)$ and $F'(\eta)$, $G'(\eta)$ at fixed parameters $\Lambda = 1$, $M = \widetilde{K} = c = 0.5$, $l = 2$, $d_n = 0.2$, $\alpha_0 = 0.8$, $h = 1$.

The effect of the unsteadiness parameter α_0 on the velocity profiles for the fluid and dust phases as a function of η, respectively, is shown in Figure 8. It is observed that the velosity profiles increase significantly as the unsteady parameter is increased. Physically, this means that with an increase in the unsteadiness parameter, the rate of sheet stretching in lateral directions increases, resulting in an increase in the velocity profiles for both the fluid and dust phases.

Thus, using the obtained analytical results, one can quickly and easily provide a physical interpretation of the processes caused by variations in various parameters on the flow of a nanofluid containing dust particles without using any numerical techniques.

There are many types of studies that give numerical results of the problem under consideration, but with fewer physical effects. The analytical results obtained from the expressions (21) for the local skin friction coefficients $-f''(0)$, $-g''(0)$ under conditions,

$$\alpha_0 = 0, \quad \widetilde{K} = 0, \quad \phi_s = 0, \quad \beta_v = 0$$

can be compared to the known numerical results of Ahmad and Nazar [32], Nadeem et al. [33], Vajravelu et al. [34], and Oyelakin et al. [19]. Table 2 shows that a good agreement is established between the exact solution (20) and the available numerical results [19, 32–34].

In the case of the flow of a Newtonian electrically conductive fluid with dust particles under the conditions,

$$\alpha_0 = 0, \quad c = 0, \quad \widetilde{K} = 0, \quad \phi_s = 0,$$

we obtain an exact analytical expression for the coefficient of skin friction, which coincides with the result of Jalil et al. [26]:

$$-f''(0) = \sqrt{1 + M + \frac{\beta_v l}{1 + \beta_v}}. \tag{37}$$

The analytical results obtained as a result of the use of expression (37) are perfectly consistent with the numerical results of Gireesha et al. [35].

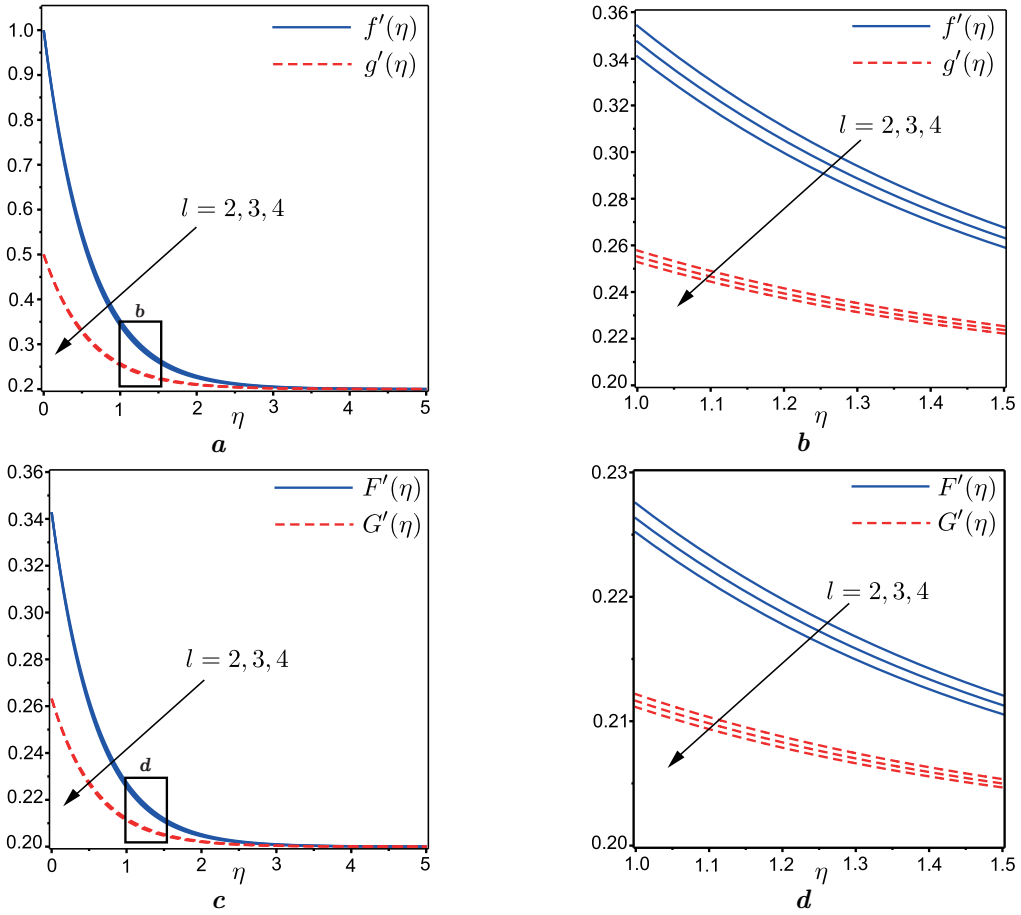

Fig. 6. Effect of l on velocity profiles $f'(\eta)$, $g'(\eta)$ and $F'(\eta)$, $G'(\eta)$ at fixed parameters $\Lambda = 1$, $M = \widetilde{K} = c = 0.5$, $d_n = 0.2$, $\alpha_0 = 0.8$, $h = 1$, $\beta_v = 0.3$.

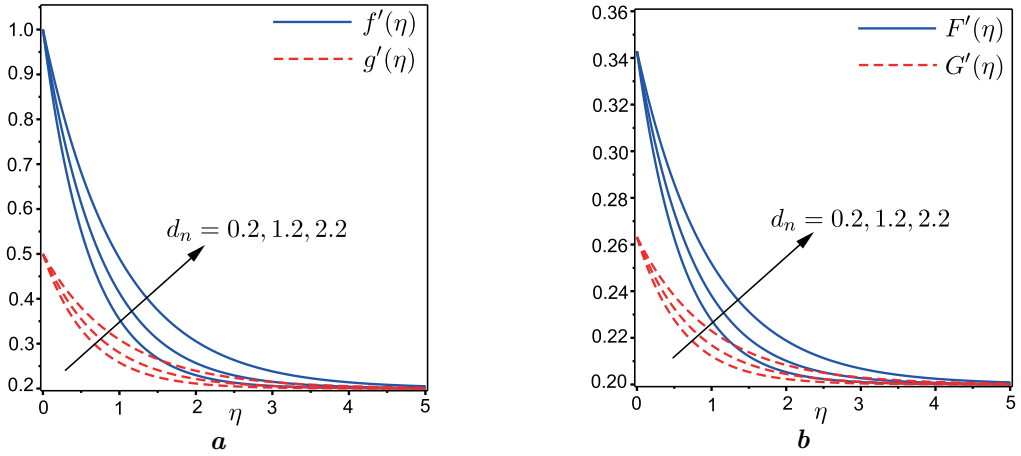

Fig. 7. Effect of d_n on velocity profiles $f'(\eta)$, $g'(\eta)$ and $F'(\eta)$, $G'(\eta)$ at fixed parameters $\Lambda = 1$, $M = \widetilde{K} = c = 0.5$, $l = 2$, $\alpha_0 = 0.8$, $h = 1$, $\beta_v = 0.3$.

In the case of the flow of a non-Newtonian electrically conductive nanofluid with dust particles under the conditions,

$$\alpha_0 = 0, \quad c = 0, \quad \widetilde{K} = 0,$$

we obtain an exact analytical expression for the coefficient of skin friction, which coincides with the result of Khan et al. [30]:

$$-f''(0) = \sqrt{\frac{1}{\left(1 + \frac{1}{\Lambda}\right)\frac{\mu_{nf}}{\mu_f}} \left(\frac{\rho_{nf}}{\rho_f} + \frac{\sigma_{nf}}{\sigma_f} M + \frac{\beta_v l}{1 + \beta_v} \right)}. \tag{38}$$

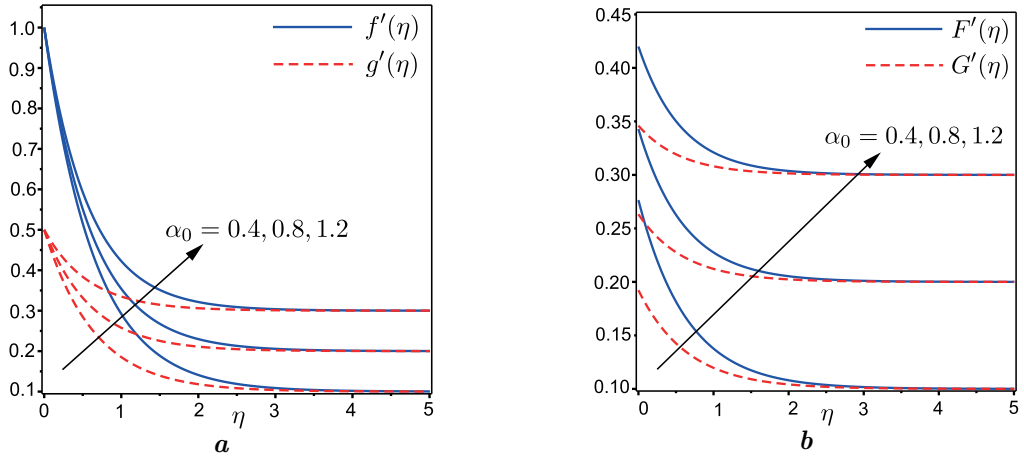

Fig. 8. Effect of α_0 on velocity profiles $f'(\eta)$, $g'(\eta)$ and $F'(\eta)$, $G'(\eta)$ at fixed parameters $\Lambda = 1$, $M = \widetilde{K} = c = 0.5$, $l = 2$, $d_n = 0.2$, $h = 1$, $\beta_v = 0.3$.

As shown in [30], the analytical results obtained by using the expression (38) are in complete agreement with the numerical results of Vajravelu et al. [34].

Table 3. Values $-f''(0)$ and $g''(0)$ for the unsteady flow of a dusty nanofluid with various variations of parameters.

Λ	M	$\widetilde{K}$	β_v	l	d_n	$-f''(0)$	$-g''(0)$
1	0.5	0.5	0.3	2	0.2	1.3173	0.4939
3	0.5	0.5	0.3	2	0.2	1.6133	0.6050
∞	0.5	0.5	0.3	2	0.2	1.8629	0.6986
1	1.5	0.5	0.3	2	0.2	1.4676	0.5507
1	2.5	0.5	0.3	2	0.2	1.6058	0.6022
1	0.5	1.5	0.3	2	0.2	1.4336	0.5376
1	0.5	2.5	0.3	2	0.2	1.5412	0.5779
1	0.5	0.5	0.5	2	0.2	1.3563	0.5088
1	0.5	0.5	1.0	2	0.2	1.4316	0.5368
1	0.5	0.5	0.3	3	0.2	1.3534	0.5075
1	0.5	0.5	0.3	4	0.2	1.3887	0.5207
1	0.5	0.5	0.3	2	1.2	1.0582	0.3968
1	0.5	0.5	0.3	2	2.2	0.8109	0.3040

Table 4. $-f''(0)$ and $-g''(0)$ values for various variations of the unsteadiness parameter α_0.

α_0	$-f''(0)$	$-g''(0)$
0.2	1.416173587	0.6708190675
0.4	1.390197319	0.6178654752
0.6	1.357070275	0.5587936428
0.8	1.317301918	0.4939882190
1.0	1.271313537	0.4237711790
1.2	1.219460951	0.3484174145

Next, we study the influence of the non-Newtonian (Casson) parameter Λ, the magnetic field M, the porosity $\widetilde{K}$, the fluid particle interaction parameter β_v, the mass concentration of the dust particles l, and the nanoparticle size d_n on the local skin friction coefficients $-f''(0)$, $-g''(0)$ for nanofluid Cu-H_2O. We assume that the other parameters of the problem are fixed: $\alpha_0 = 0.8$, $c = 0.5$, $\phi_s = 0.05$,

$h = 1$. Numerical values of $-f''(0)$, $-g''(0)$ for different values of Λ, M, $\widetilde{K}$, β_v, l, and d_n were obtained from exact solutions (33), (36) and presented in Table 3. From the results of Table 3, it can be seen that at the limit of the Newtonian fluid ($\Lambda = \infty$), the skin friction coefficients of the nanofluid in the x and y directions are higher compared to the non-Newtonian fluid. In addition, an increase in the parameters Λ, M, $\widetilde{K}$, β_v, and l reduces the fluid flow rate, which leads to an increase in the absolute values of the skin friction coefficients in the x and y directions. On the other hand, as nanoparticle diameter d_n increases, the coefficients of skin friction in the x and y directions decrease.

Finally, we examine the impact of the nanofluid flow's unsteadiness parameter α_0 on the local skin friction coefficients $-f''(0)$, $-g''(0)$ in the x and y directions. We assume that the other parameters of the problem are fixed:

$$\Lambda = 1, \quad M = \widetilde{K} = c = 0.5, \quad l = 2, \quad d_n = 0.2, \quad h = 1, \quad \beta_v = 0.3.$$

Using the exact solutions (33), (36), we calculate the values of the skin friction coefficients $-f''(0)$, $-g''(0)$ for various variations of the parameter α_0, which are presented in Table 4. As can be seen from the results in Table 4, an increase in the flow unsteadiness parameter leads to a decrease in the skin friction coefficients in both directions.

5. Conclusions

In the present study, for the first time, an analytical solution for a nonstationary MHD boundary flow of a Cassonian nanofluid containing dust particles over a stretching sheet is obtained. A variant of linear unsteady stretching of a sheet (see Figure 1) is considered in the lateral directions x and y. For the flow of a typical nanofluid (Cu-H_2O), analytical expressions are derived for the velocities of the fluid and dust phases as well as for skin friction in lateral directions x and y. The influence of the Casson parameter Λ, the magnetic parameter M, the porosity parameter $\widetilde{K}$, the fluid-particle interaction parameter β_v, the mass concentration of dust particles l, and nanoparticle size d_n on the velocity profiles of the fluid and dust phases is studied. New results for skin friction coefficients in lateral directions are presented in a table. For simpler physical situations, comparison of the analytical results with the numerical results of previous studies showed a high level of accuracy and consistency. The main results of this study are as follows:

1. An increase in the parameters Λ, M, $\widetilde{K}$, and l leads to a decrease in the flow rate of the fluid and dust phases.
2. It is found that the velocity of the fluid phase decreases due to an increase in the parameter β_v, while the velocity of the dust phase increases.
3. An increase in the diameter d_n of copper nanoparticles leads to a decrease in the viscosity of the water-based nanofluid and, as a consequence, an increase in the flow rates of the fluid and dust phases.
4. An increase in the unsteadiness parameter α_0 leads to an increase in the velocity profiles and a decrease in the skin friction coefficients for both fluid and dust phases in lateral directions.

This work is the basis for finding future analytical solutions that describe the unsteady three-dimensional MHD Casson flow of a dusty hybrid nanofluid or other non-Newtonian dusty fluids over a porous stretching surface.

Acknowledgements

The authors are grateful to an anonymous referee for his interest in this article and valuable comments.

[1] Saffman P. G. On the stability of laminar flow of a dusty gas. Journal of Fluid Mechanics. **13** (1), 120–128 (1962).

[2] Chakrabarti K. M. Note on boundary layer in a dusty gas. AIAA Journal. **12** (8), 1136–1137 (1974).

[3] Datta N., Mishra S. K. Boundary layer flow of a dusty fluid over a semi-infinite flat plate. Acta Mechanica. **42**, 71–83 (1982).

[4] Vajravelu K., Nayfeh J. Hydromagnetic flow of a dusty fluid over a stretching sheet. International Journal of Non-Linear Mechanics. **27** (6), 937–945 (1992).

[5] Gireesha B. J., Ramesh G. K., Lokesh H. J., Bagewadi C. S. Boundary layer flow and heat transfer of a dusty fluid over a stretching vertical surface. Applied Mathematics. **2** (4), 475–481 (2011).

[6] Gireesha B. J., Roopa G. S., Lokesh H. J., Bagewadi C. S. MHD flow and heat transfer of a dusty fluid over a stretching sheet. International Journal of Physical and Mathematical Sciences. **3**, 171–182 (2012).

[7] Gireesha B. J., Venkatesh P., Shashikumar N. S., Prasannakumara B. C. Boundary layer flow of dusty fluid over a radiating stretching surface embedded in a thermally stratified porous medium in the presence of uniform heat source. Nonlinear Engineering. **6** (1), 31–41 (2017).

[8] Sakiadis B. C. Boundary layer behavior on continuous solid surfaces. II. The boundary layer on a continuous flat surface. AIChE Journal. **7** (2), 221–225 (1961).

[9] Tsou F. K., Sparrow E. M., Goldstein R. J. Flow and heat transfer in the boundary layer on a continuous moving surface. International Journal of Heat and Mass Transfer. **10** (2), 219–235 (1967).

[10] Crane L. Flow past a stretching plate. Zeitschrift für Angewandte Mathematik und Physik. **21**, 645–647 (1970).

[11] Bhattacharyya K. Boundary Layer Stagnation-Point Flow of Casson Fluid and Heat Transfer Towards a Shrinking/Stretching Sheet. Frontiers in Heat and Mass Transfer. **4** (2), 023003 (2013).

[12] Mukhopadhyay S., De P. R., Bhattacharyya K., Layek G. C. Casson Fluid Flow Over an Unsteady Stretching Surface. Ain Shams Engineering Journal. **4** (4), 933–938 (2013).

[13] Nandy S. K. Analytical Solution of MHD Stagnation-Point Flow and Heat Transfer of Casson Fluid Over a Stretching Sheet with Partial Slip. International Scholarly Research Notices. **2013**, 108264 (2013).

[14] Nadeem S., Haq R. U., Akbar N. S., Khan Z. H. MHD three-dimensional Casson fluid flow past a porous linearly stretching sheet. Alexandria Engineering Journal. **52** (4), 577–582 (2013).

[15] Nadeem S., Haq R. U., Akbar N. S. MHD three-dimensional boundary layer flow of Casson nanofluid past a linearly stretching sheet with convective boundary condition. IEEE Transactions on Nanotechnology. **13** (1), 108–115 (2014).

[16] Mahanta G., Shaw S. 3D Casson fluid flow past a porous linearly stretching sheet with convective boundary condition. Alexandria Engineering Journal. **54** (3), 653–659 (2015).

[17] Krishna Murthy M. Analytical Solution for MHD Casson Fluid Flow Past a Porous Linearly Stretching Surface with Wall Mass Transfer. Chemical and Process Engineering Research. **41**, 29–37 (2016).

[18] Choi S. U. S., Eastman J. A. Enhancing thermal conductivity of fluids with nanoparticles. Am. Soc. Mech. Eng. Fluids Eng. Div. FED. **231**, 99–105 (1995).

[19] Oyelakin I. S., Mondal S., Sibanda P. Unsteady MHD three-dimensional Casson nanofluid flow over a porous linear stretching sheet with slip condition. Frontiers in Heat and Mass Transfer. **8** (1), 37 (2017).

[20] Madhusudan S., Kharabela S., Kumar P. S. Numerical analysis of three-dimensional MHD flow of Casson nanofluid past an exponentially stretching sheet. Karbala International Journal of Modern Science. **6** (1), 93–102 (2020).

[21] Ibrahim W., Anbessa T. Three-Dimensional MHD Mixed Convection Flow of Casson Nanofluid with Hall and Ion Slip Effects. Hindawi Mathematical Problems in Engineering. **2020**, 8656147 (2020).

[22] Japili N., Rosali H., Bachok N. MHD stagnation point flow over a stretching or shrinking sheet in a porous medium with velocity slip. Mathematical Modeling and Computing. **9** (4), 825–832 (2022).

[23] Yahaya R. I., Ali F. M., Arifin N. M., Khashi'ie N. S., Isa S. S. P. M. MHD flow of hybrid nanofluid past a stretching sheet: double stratification and multiple slips effects. Mathematical Modeling and Computing. **9** (4), 871–881 (2022).

[24] Alias N. S., Hafidzuddin M. E. H. Effect of suction and MHD induced Navier slip flow due to a non-linear stretching/shrinking sheet. Mathematical Modeling and Computing. **9** (1), 83–91 (2022).

[25] Nithya N., Vennila B. MHD Nanofluid boundary layer flow over a stretching sheet with viscous, ohmic dissipation. Mathematical Modeling and Computing. **10** (1), 195–203 (2023).

[26] Jalil M., Asghar S., Yasmeen Sh. An Exact Solution of MHD Boundary Layer Flow of Dusty Fluid over a Stretching Surface. Mathematical Problems in Engineering. **2017**, 2307469 (2017).

[27] Vishalakshi A. B., Mahabaleshwar U. S., Sarris I. E. An MHD Fluid Flow over a Porous Stretching/Shrinking Sheet with Slips and Mass Transpiration. Micromachines. **13** (1), 116 (2022).

[28] Mahabaleshwar U. S., Anusha T., Laroze D., Said N. M., Sharifpur M. An MHD Flow of Non-Newtonian Fluid Due to a Porous Stretching/Shrinking Sheet with Mass Transfer. Sustainability. **14** (12), 7020 (2022).

[29] Vishalakshi A. B., Mahabaleshwar U. S., Hatami M. MHD Casson carbon nanotube flow with mass and heat transfer under thermosolutal Marangoni convection in a porous medium: analytical solution. Scientific Reports. **12**, 16071 (2022).

[30] Khan U., Mebarek-Oudina F., Zaib A., Ishak A., Abu Bakar S., Sherif E.-S. M., Baleanu D. An exact solution of a Casson fluid flow induced by dust particles with hybrid nanofluid over a stretching sheet subject to Lorentz forces. Waves in Random and Complex Media (2022).

[31] Akbar A. A., Ahammad N. A., Awan A. U., Hussein A. K., Gamaoun F., Tag-ElDin E. M., Ali B. Insight into the Role of Nanoparticles Shape Factors and Diameter on the Dynamics of Rotating Water-Based Fluid. Nanomaterials. **12** (16), 2801 (2022).

[32] Ahmad K., Nazar R. Magnetohydrodynamic three-dimensional flow and heat transfer over a stretching surface in a viscoelastic fluid. Journal of Science and Technology. **3** (1), 33–46 (2011).

[33] Nadeem S., Haq R. U., Akbar N. S., Khan Z. H. MHD three-dimensional Casson fluid flow past a porous linearly stretching sheet. Alexandria Engineering Journal. **52** (4), 577–582 (2013).

[34] Vajravelu K., Prasad K., Vaidya H., Basha N. Z., Ng C.-O. Mixed convective flow of a Casson fluid over a vertical stretching sheet. International Journal of Applied and Computational Mathematics. **3**, 1619–1638 (2017).

[35] Gireesha B. J., Ramesh G. K., Bagewadi C. S. Heat transfer in MHD flow of a dusty fluid over a stretching sheet with viscous dissipation. Advances in Applied Science Research. **3** (4), 2392–2401 (2012).

Точний розв'язок для нестаціонарного тривимірного магнітогідродинамічного потоку Кассона запиленої нанорідини над пористим листом, що розтягується

Копп М. Й.[1], Яновський В. В.[1,2]

[1] *Інститут монокристалів, Національна академія наук України, пр. Науки 60, 61072 Харків, Україна*
[2] *Харківський національний університет імені В. Н. Каразіна, майдан Свободи, 4, 61022, Харків, Україна*

Досліджено нестаціонарний тривимірний (3D) потік Кассона нанорідини, що містить частинки пилу, над пористим листом, який лінійно розтягується, у присутності зовнішнього магнітного поля. Вважається, що лист розтягнутий в обох напрямках вздовж площини xy. Керівними рівняннями двофазної моделі є диференціальні рівняння в частинних похідних, які перетворюються на звичайні рівняння за допомогою перетворень подібності. Нанорідина є суспензію наночастинок на водній основі. У цьому дослідженні розглянуто, як розмір наночастинок впливає на властивості потоку пилової нанорідини. Математична модель містить базові рівняння для рідинної та пилової фаз у формі тривимірних диференціальних рівнянь у частинних похідних, які за допомогою відповідного перетворення подібності перетворюються на безрозмірні звичайні розмірні рівняння. Отримано точний аналітичний розв'язок цієї крайової задачі. Детально обговорюється вплив різних фізичних величин на швидкість пилу та нанорідини, включаючи параметр Кассона, магнітний параметр, параметр пористості, параметр взаємодії рідини та частинок, масову концентрацію частинок пилу та розмір наночастинок. У декількох конкретних випадках поточне аналітичний розв'язок демонструє добру згоду з раніше опублікованими чисельними дослідженнями.

Ключові слова: *лист, що розтягується; нестаціонарний тривимірний (3D) потік Кассона; нанорідина; частинки пилу; діаметр наночастинок; сила Лоренца*